RUC

Roskilde University

Novel Characteristics of Valveless Pumping

Timmermann, Stine; Ottesen, Johnny T.

Published in:
Physics of Fluids

DOI:
10.1063/1.3114603

Publication date:
2009

Document Version
Publisher's PDF, also known as Version of record

Citation for published version (APA):
Timmermann, S., & Ottesen, J. T. (2009). Novel Characteristics of Valveless Pumping. *Physics of Fluids*, *21*(5). https://doi.org/10.1063/1.3114603

General rights
Copyright and moral rights for the publications made accessible in the public portal are retained by the authors and/or other copyright owners and it is a condition of accessing publications that users recognise and abide by the legal requirements associated with these rights.

- Users may download and print one copy of any publication from the public portal for the purpose of private study or research.
- You may not further distribute the material or use it for any profit-making activity or commercial gain.
- You may freely distribute the URL identifying the publication in the public portal.

Take down policy
If you believe that this document breaches copyright please contact rucforsk@kb.dk providing details, and we will remove access to the work immediately and investigate your claim.

Download date: 05. May. 2023

Novel characteristics of valveless pumping

S. Timmermann and J. T. Ottesen[a)]
Department of Sciences, Mathematics and Physics, Roskilde University, P.O. Box 260, Roskilde 4000, Denmark

(Received 30 October 2007; accepted 22 December 2008; published online 4 May 2009)

This study investigates the occurrence of valveless pumping in a fluid-filled system consisting of two open tanks connected by an elastic tube. We show that directional flow can be achieved by introducing a periodic pinching applied at an asymmetrical location along the tube, and that the flow direction depends on the pumping frequency. We propose a relation between wave propagation velocity, tube length, and resonance frequencies associated with shifts in the pumping direction using numerical simulations. The eigenfrequencies of the system are estimated from the linearized system, and we show that these eigenfrequencies constitute the resonance frequencies and the horizontal slope frequencies of the system; "horizontal slope frequency" being a new concept. A simple model is suggested, explaining the effect of the gravity driven part of the oscillation observed in response to the tank and tube diameter changes. Results are partly compared with experimental findings. © *2009 American Institute of Physics*. [DOI: 10.1063/1.3114603]

I. INTRODUCTION

Generally valveless pumping is classified as directional flow in a system of valveless fluid-filled flexible tubes, where an applied periodic force (a device compressing one of the tubes) generates a frequency dependent unidirectional flow in the system. The phenomena of valveless pumping have been investigated using a number of approaches and methods. The studies of the most prominent systems include flow in the annulus and the open tank system. The annulus consists of two or more flexible tubes with different elasticities, connected in a closed circuit. In the literature, this system has been described both with ordinary differential equation (ODE) (Refs. 1 and 2) and partial differential equation (PDE) (Refs. 3–7) models. Yet another approach is to simulate the flow using molecular dynamics techniques.[8,9] The open tank system consists of two tanks connected by a flexible tube. This system has been investigated using models based on Navier–Stokes equations.[10–14] A variation of the open tank system is the T-pipe system in which the tanks are connected by a rigid T-pipe with a piston placed in the "leg" of the T-pipe. The flow in this system has been studied using ODE models.[15,16] Both experiments and modeling approaches confirm the phenomena and show the same characteristic features of valveless flow: The magnitude and the direction of the flow depend in a complex way on the pumping frequency and amplitude, the pump duty cycle, and the system material properties and dimensions, e.g., tube radius.

The valveless flow phenomenon is universal in the sense that it is scale invariant and qualitatively independent of topology. However, despite agreement between the various studies, a full understanding of the mechanisms responsible for the phenomenon has not yet been obtained.

In this paper we add to the understanding of the mechanisms responsible for valveless flow by investigating valveless flow in the open tank system, shown in Fig. 1. Reference 10 completed a numerical investigation of this system. He observed flow reversals in the system and found that the flow reversals depend on the pumping frequency and the tube length. However, the study did not uncover the mechanisms responsible for the phenomenon. Reference 12 used a more advanced numerical scheme to investigate the same system of equations, but with modified boundary conditions. They showed that valveless flow can be obtained both in the original nonlinear model and in a linearized model with friction. However their work is not focused on how the system depends on the pumping frequency. Reference 14 showed that a mismatch of characteristic impedance between the flow channels is necessary for creating wave reflection sites in a variant of the system. They also present results of an experimental study that demonstrate the phenomena. Inspired by Refs. 11 and 12, we propose a one-dimensional (1D) model derived from the Navier–Stokes equation for flow in a tube. In order to write the equations on a generalized conservation form, we formulate the model in velocity and cross-sectional area instead of velocity and pressure as was done in previous studies. The boundary equations describing the fluid in the tanks are derived from the instationary Bernoulli equation as proposed by Ref. 10 but in contrast to Refs. 12 and 14. Mathematically, this formulation turns out to be a more natural way of connecting the tube and the tanks. Although valveless pumping has been detected in this system by others, the mechanisms behind the phenomenon have not yet been provided.

In this paper, we show that there are two qualitatively different ways that pumping reversal can occur: At "resonance points," where pumping reversal appear to be connected with the resonance in the system, and at "zero points," which are not connected with resonance. Furthermore, zero points appear to be influenced by the position of the pump, in contrast to resonance points. Based on numerical simulations we propose a relation between resonance

a)Telephone: (+45) 4674 2298. Fax: (+45) 4674 3020. Electronic mail: johnny@ruc.dk.

 © 2009 American Institute of Physics

Downloaded 05 Jan 2010 to 130.226.199.115. Redistribution subject to AIP license or copyright; see http://pof.aip.org/pof/copyright.jsp

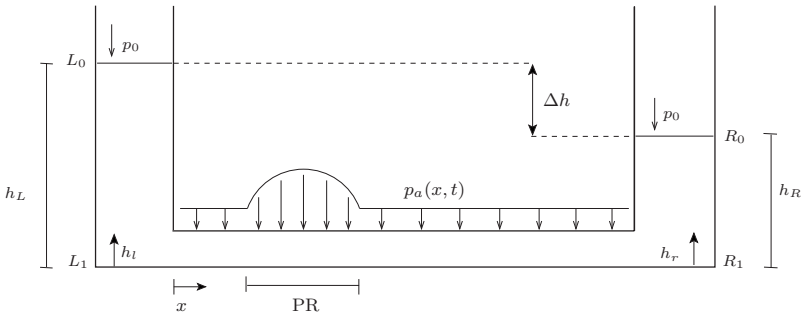

FIG. 1. Two fluid-filled tanks connected by a flexible rubber tube. Periodic compression at an asymmetric location of the rubber tube generates a difference in fluid levels, $\Delta h = h_L - h_R$. Compression is obtained by varying the external pressure $p_a(x,t)$ in the pump region (PR) (enhanced online) [URL: http://dx.doi.org/10.1063/1.3114603.1].

points, wave propagation velocity, and tube length. Furthermore, using a linearized model, we show that the eigenfrequencies define two series of frequencies; resonance frequencies and horizontal slope frequencies. The resonance frequencies agree with the resonance points whereas the horizontal slope frequencies constitute a new concept. Additionally, to understand the system thoroughly we analyze the gravity driven component separately. This analysis shows how the period of the gravitational oscillations depends on the ratio between the cross-sectional diameters of the tube and tanks.

II. EXPERIMENTAL SETUP

To illustrate valveless pumping we carried out a series of experiments in an open tank system, see Fig. 1. This system comprises an elastic silicone rubber tube with wall thickness of 0.004 m, length of 1.8 m, and rest diameter of 0.03 m, i.e., at zero transmural pressure, and Young modulus 4.033×10^6 kg/ms^2 connected to two identical open rigid tanks. The diameter of the tanks was 5.7 times the rest diameter of the tube. The system was filled with water to the level of one meter in the tanks. Valveless flow was obtained by compressing a piston from above, as shown in Fig. 2(a). The piston compressed the tube at frequencies ranging from 0–5 Hz.

Pumping at a given frequency makes the fluid flow from one tank to the other. This net change in fluid continues until the force generated by the pump is balanced by the gravitational force. At this point a "steady state" is reached and a water level difference between the tanks is created. At steady state the water level oscillates with the pumping frequency. The resulting water level depends on the frequency and the location of the pump. Furthermore, we noted that changing the frequency or the location of the pump may reverse the flow, and consequently the elevated water level shifts from one tank to the other.

In the experiment we measured the resonance frequencies and the water level in the tanks. The tank water level was measured continuously using a high speed video camera. Experiments were carried out for pumping frequencies ranging from 0 to 5 Hz. In a separate experiment, we measured the water level in the tank as a function of time without compressing the tube but starting with an elevated water level in one of the tanks. The result is smooth damped sinus-like waves. When measuring the period of the gravity driven oscillations, the average was calculated over as many periods as possible (which was at least four to five periods) to improve accuracy. Video recordings of the experimental setup for some of the experiments can be found in the online version by clicking on Fig. 1.

The focus of this paper is on understanding the system through mathematical modeling and, therefore, we will not go into further details with the experiment. However, we will refer to the experiment and some of the experimental results obtained for validation and discussion of the model.

III. ONE-DIMENSIONAL MATHEMATICAL MODEL OF THE SYSTEM

A. The tube

Consider the fluid-filled system illustrated in Fig. 1. The motion of a fluid is described by the Navier–Stokes equations. The derivation of the 1D model is based on the assumptions of constant temperature, incompressible Newtonian fluid, irrotational, and axisymmetric flow. Equations are derived using a velocity profile described by a general power law characterized by γ. We chose $\gamma = 2$ in the simulations, which gives a parabolic velocity profile (increasing values of γ gives flatter and flatter velocity profiles). With these assumptions, the model equations become

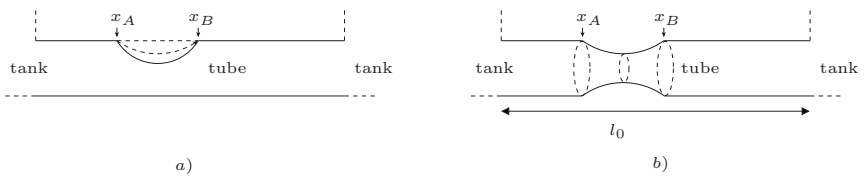

FIG. 2. (a) The axial nonsymmetrical compression of the tube between x_A and x_B as in the experiment. (b) In the model, the tube is compressed axial symmetrically between x_A and x_B.

Downloaded 05 Jan 2010 to 130.226.199.115. Redistribution subject to AIP license or copyright; see http://pof.aip.org/pof/copyright.jsp

$$\frac{\partial}{\partial t}\begin{pmatrix} A \\ u \end{pmatrix} + \frac{\partial}{\partial x}\begin{pmatrix} uA \\ \frac{1}{2}u^2 + \frac{1}{\rho}p_t \end{pmatrix} = \begin{pmatrix} 0 \\ -\frac{1}{\rho}\frac{\partial p_a}{\partial x} - \frac{\mu}{\rho}2\pi(\gamma+2)\frac{u}{A} \end{pmatrix}. \tag{1}$$

Here A denotes the cross-sectional area of the tube, u denotes the 1D velocity in the longitudinal direction, and $p_t = p(A) - p_a$ denotes the transmural pressure, where p is the pressure in the tube and p_a is the external pressure. These quantities are all functions of the position along the tube x and time t. The parameters ρ and μ are assumed constant and denote density and viscosity of the fluid, respectively. A detailed derivation of the governing equations can be found in Ref. 5.

The transmural pressure and the cross-sectional area are related by

$$p_t(A) = \frac{4}{3}\frac{sE}{r_{\text{rest}}}\left(1 - \sqrt{\frac{A_{\text{rest}}}{A}}\right), \tag{2}$$

where E denotes Young modulus of the tube wall, r_{rest} denotes the rest radius (corresponding to A_{rest}), A denotes the cross-sectional area of the tube, and s denotes the wall thickness of the tube. This constitutive equation has been used in previous studies concerning blood motion in vessels, see Ref. 17 for further discussion, but it deviates from the one used by Refs. 10 and 12.

The wave propagation velocity $c_\pm = u \pm a$, where $a = \sqrt{(4/3)(sE/\rho D_{\text{rest}})}\sqrt[4]{A_{\text{rest}}/A}$ can be found by calculating eigenvalues of the coefficient matrix when the system of equations is placed in the form

$$\frac{\partial}{\partial t}\begin{pmatrix} A \\ u \end{pmatrix} + \begin{pmatrix} u & A \\ \frac{4}{3}\frac{sE}{\rho D_{\text{rest}}}\sqrt{\frac{A_{\text{rest}}}{A^3}} & u \end{pmatrix}\frac{\partial}{\partial x}\begin{pmatrix} A \\ u \end{pmatrix} = \begin{pmatrix} 0 \\ -\frac{1}{\rho}\frac{\partial pa}{\partial x} - \frac{\mu}{\rho}2\pi(\gamma+2)\frac{u}{A} \end{pmatrix}. \tag{3}$$

If the external pressure equals the inner pressure, i.e., $A = A_{\text{rest}}$, the wave propagation velocity is reduced to the constant velocity $a_0 = \sqrt{4sE/3\rho D_{\text{rest}}}$, the well known Moens–Korteweg approximation.[18] Substituting a_0 into the system of equations simplifies the equations as

$$\frac{\partial}{\partial t}\begin{pmatrix} A \\ u \end{pmatrix} + \frac{\partial}{\partial x}\begin{pmatrix} Au \\ \frac{1}{2}u^2 + 2a_0^2\left(1 - \sqrt{\frac{A_{\text{rest}}}{A}}\right) \end{pmatrix} = \begin{pmatrix} 0 \\ -\frac{1}{\rho}\frac{\partial p_a}{\partial x} - \frac{\mu}{\rho}2\pi(\gamma+2)\frac{u}{A} \end{pmatrix}. \tag{4}$$

In the physical experiment we used a piston to compress the tube, as shown in Fig. 2(a), violating the axial symmetrical condition. In contrast to this the pump in the model is described by axial symmetric compression, obtained by imposing an oscillating external pressure, as indicated in Fig. 2(b). The external pressure is described by the C^1-function,

$$p_a(x,t) = \begin{cases} p_0\left\{1 + \eta\dfrac{(x-x_A)^2(x_B-x)^2}{\left[\frac{1}{2}(x_B-x_A)\right]^4}\sin(2\pi\nu t)\right\} & \text{for } x \in [x_A, x_B], \\ p_0 & \text{else}, \end{cases} \tag{5}$$

$p_0(1+\eta)$ being the maximal external pressure applied to the tube and ν the frequency of compression. The constant external pressure p_0 is set to atmospheric pressure. This pump function is a moderation of the function used in Ref. 12. The function has been altered in order to give a C^1-function.

B. Boundary and initial conditions

The relation between the flow across the two tube ends and the fluid levels in the two tanks are described by boundary conditions. For each boundary, two additional differential equations are needed to close the system of equations. For both left and right boundaries the additional equations are obtained from the instationary Bernoulli equation.

Boundary conditions are obtained by solving the instationary Bernoulli equation along a streamline in the tank,[19] a mechanical energy balance for isothermal conduit flow,

$$\nabla\left(\frac{\partial \phi}{\partial t} + \frac{1}{2}u^2 + \frac{1}{\rho}p + gh\right) = 0, \tag{6}$$

where ϕ denotes the scalar potential function. Thus

$$\frac{1}{2}u_{L_1}^2 + \frac{p_{L_1}}{\rho} = -\int_0^{h_L}\frac{\partial u}{\partial t}dh + \frac{1}{2}u_{L_0}^2 + \frac{p_{L_0}}{\rho} + gh_L, \tag{7}$$

by integration from $L_1 = 0$ to $L_0 = h_L$, where h_L is the height of the water level. Note that $u_{L_1} = u(0,t)$ and $u_{L_0} = u(h_L,t)$ and similarly for the pressures. To eliminate u_{L_0} we apply the continuity equation $A_{\text{tank}}u_{L_0} = A_{L_1}u_{L_1}$ and to avoid time dependence, we approximate A_{L_1} by A_{start}, where A_{start} being the

Downloaded 05 Jan 2010 to 130.226.199.115. Redistribution subject to AIP license or copyright; see http://pof.aip.org/pof/copyright.jsp

initial cross-section area at hydrostatic pressure, derived in Eq. (13) below.

Thus the following approximation for the first term on the right hand side of Eq. (7) holds, i.e.,

$$\int_0^{h_L} \frac{\partial u}{\partial t} dh \approx \int_0^{h_L} \frac{\frac{\partial u_{L_1}}{\partial t} + \frac{\partial u_{L_0}}{\partial t}}{2} dh \approx \frac{1}{2} \frac{du_{L_1}}{dt} \left(1 + \frac{A_{\text{start}}}{A_{\text{tank}}}\right) h_L. \tag{8}$$

Energy is dissipated when fluid flows from one tube to the other and therefore slows down the flow. To avoid modeling the minor regions of turbulent flow at the connection between the tanks and the tube explicitly, the energy loss is modeled assuming that it is proportional to the squared flow velocity with proportionality constant ξ. Consequently, the term $\frac{1}{2}(u_{L_1})^2$ in Eq. (7) is replaced by $\frac{1}{2}(1+\xi)(u_{L_1})^2$. Numerical simulations comparing this simplified treatment of energy loss to the loss term $\frac{1}{2}[1+\text{sign}(u_{L_1})]$, as used in Refs. 11, 20, and 12, showed no significant difference. Hence we proceed with our simpler choice.

The final boundary conditions for the left boundary are obtained by rewriting the inner pressure p_{L_1} using Eq. (2) as

$$\frac{du_{L_1}}{dt} = \frac{1}{\left(1 + \frac{A_{\text{start}}}{A_{\text{tank}}}\right) h_L} \left[\left(\left(\frac{A_{L_1}}{A_{\text{tank}}} \right)^2 - (1+\xi) \right) u_{L_1}^2 - 4a_0^2 \left(1 - \sqrt{\frac{A_{\text{rest}}}{A_{L_1}}} \right) + 2gh_L \right]. \tag{9}$$

As a result, the change in the fluid level in the left tank is given by the velocity of the fluid at the top of the tank, and using the continuity equation we get the second boundary condition for the left boundary,

$$\frac{dh_L}{dt} = -\frac{A_{L_1}}{A_{\text{tank}}} u_{L_1}. \tag{10}$$

The boundary conditions for the right boundary are similar to those of the left boundary except that one has to substitute the indices L and L_1 by R and R_1, respectively, and change the sign of the derivatives [see Eqs. (20) and (21) below].

Note that $A_{L_1}=A(0,t)$ and $A_{R_1}=A(l,t)$ are determined by Eq. (2) and consequently these quantities are time dependent. This time dependence is important since boundary conditions derived from assuming constant cross-sectional area for instance, causes rarefractions created by the numerical method.[21,5] Furthermore, such boundary conditions simply shift the mechanistic peculiarity (that neighboring elements of the discretized equation form might have different cross-sectional areas (without leaking) at the connection between the tank and the tube further down the tube.

At time $t=0$ the system is in equilibrium. Thus $h_L(t=0)=h_R(t=0)=h_0$. Assuming that the fluid height h_0 is larger than the diameter of the tube, the fluid in the tanks will impose a positive transmural pressure on the tube causing an expansion of the cross-sectional area of the tube. Thus, the hydrostatic pressure determines the pressure and, consequently, the initial cross-sectional area of the tube,

$$p_t(x,0) = \rho g h_0 \Leftrightarrow A(x,0) = A_{\text{rest}} \left(1 - \frac{gh_0}{2a_0^2}\right)^{-2}. \tag{11}$$

Imposing these conditions gives initial conditions on the form

$$u(x,0) = 0, \tag{12}$$

$$A(x,0) = A_{\text{start}} = A_{\text{rest}} \left(1 - \frac{gh_0}{2a_0^2}\right)^{-2}. \tag{13}$$

C. The 1D model in dimensionless form

We introduce nondimensional variables in order to simplify the numerical solutions of the equations. To do so, we use the following characteristic quantities: the rest radius r_0 (i.e., radius at zero transmural pressure) and the average fluid velocity u_0. We define nondimensional variables (indicated by $\tilde{}$),

$$\tilde{x} = \frac{x}{r_0}, \quad \tilde{t} = \frac{u_0}{r_0} t, \quad \tilde{u} = \frac{u}{u_0}, \quad \tilde{A} = \frac{A}{r_0^2}, \tag{14}$$

where $\tilde{x}$, $\tilde{t}$, $\tilde{u}$, and $\tilde{A}$ are the dimensionless space, time, velocity, and cross-sectional area variables, respectively. To simplify the system of equations we let

$$\tilde{p} = \frac{p}{\rho u_0^2}, \quad \tilde{\nu} = \frac{r_0}{u_0} \nu, \quad \tilde{h} = \frac{h}{r_0}, \quad \tilde{A}_{\text{tank}} = \frac{A_{\text{tank}}}{r_0^2}, \quad \tilde{A}_{\text{start}} = \frac{A_{\text{start}}}{r_0^2}, \tag{15}$$

where $\tilde{p}$, $\tilde{\nu}$, $\tilde{h}$, $\tilde{A}_{\text{tank}}$, and $\tilde{A}_{\text{start}}$ are the dimensionless pressure, pumping frequency, water level, cross-sectional area of the tanks, and cross-sectional area of the tube at $t=0$, respectively. Introducing the Reynolds number ($\text{Re}=\rho u_0 r_0/\mu$) and the Froude number ($\text{Fr}=u_0^2/gr_0$) the systems of equations, boundary and initial conditions reduce to (now omitting the $\tilde{}$).

Tube:

$$\frac{\partial}{\partial t}\begin{pmatrix} A \\ u \end{pmatrix} + \frac{\partial}{\partial x}\begin{pmatrix} Au \\ \frac{1}{2}u^2 + 2\frac{a_0^2}{u_0^2}\left(1 - \sqrt{\frac{A_{\text{rest}}}{A}}\right) \end{pmatrix} = \begin{pmatrix} 0 \\ -\frac{\partial p_a}{\partial x} - \frac{2(\gamma+2)\pi}{\text{Re}} \frac{u}{A} \end{pmatrix}. \tag{16}$$

Pump:

Downloaded 05 Jan 2010 to 130.226.199.115. Redistribution subject to AIP license or copyright; see http://pof.aip.org/pof/copyright.jsp

$$p_a(x,t) = \begin{cases} p_0\left\{1 + \eta \dfrac{(x-x_A)^2(x_B-x)^2}{\left[\frac{1}{2}(x_B-x_A)\right]^4}\sin(2\pi\nu t)\right\} & \text{for } x \in [x_A, x_B], \\ p_0 & \text{else.} \end{cases} \tag{17}$$

Left boundary condition:

$$\frac{du_L}{dt} = \frac{1}{\left(1+\frac{A_{\text{start}}}{A_{\text{tank}}}\right)h_L}\left[\left(\frac{A_L}{A_{\text{tank}}} - (1+\xi)\right)u_L^2 - 4\frac{a_0^2}{u_0^2}\left(1 - \sqrt{\frac{A_{\text{rest}}}{A_L}}\right) + \frac{2h_L}{\text{Fr}}\right], \tag{18}$$

$$\frac{dh_L}{dt} = -\frac{A_L}{A_{\text{tank}}}u_L. \tag{19}$$

Right boundary condition:

$$\frac{du_R}{dt} = \frac{-1}{\left(1+\frac{A_{\text{start}}}{A_{\text{tank}}}\right)h_R}\left[\left(\frac{A_R}{A_{\text{tank}}} - (1+\xi)\right)u_R^2 - 4\frac{a_0^2}{u_0^2}\left(1 - \sqrt{\frac{A_{\text{rest}}}{A_R}}\right) + \frac{2h_R}{\text{Fr}}\right], \tag{20}$$

$$\frac{dh_R}{dt} = \frac{A_R}{A_{\text{tank}}}u_R. \tag{21}$$

Initial conditions:

$$u(x,0) = 0, \tag{22}$$

$$A(x,0) = A_{\text{rest}}\left(1 - \frac{u_0^2}{2a_0^2}\frac{h_0}{\text{Fr}}\right)^{-2}. \tag{23}$$

Together, these equations constitute the distributed 1D model of the open tank system.

IV. NUMERICAL METHODS

The system of equations is solved using a second order finite difference method. For the tube we discretize the equations using the MacCormack scheme[22] and to evaluate the boundary conditions (the equations for the tanks) we use the method of characteristics. As shown in Ref. 7 differences between the three second order schemes, LaxWendroff, MacCormack, and dissipative relation preserving methods, are minor for flows in an elastic tube. Other choices could be finite element methods,[14] spectral methods or combinations of the two methods.[23] Finite element methods work well but have some unresolved mathematical problems when applied to Navier–Stokes' equations,[24] and the spectral method was originally designed for smooth solutions with periodic boundary conditions. The MacCormack scheme was implemented in MATLAB 6.5 under Debian GNU/Linux on a workstation. The dimensionless equations were solved on a lattice in the (x,t) plane with the spatial domain $[0,l_0]=[0,1.8]$ m divided into $J=200$ intervals. This discretization leads to a dimensionless step size $\Delta x=0.6$ (corresponding to 9×10^{-3} m) and the time domain was discretized by a dimensionless time step $\Delta t=10^{-3}$ (corresponding to 7.5×10^{-5} s). The height difference corresponding to 60 s range was computed in 12 min while a whole frequency scan (0.5–15 Hz) took approximately 10 h of CPU time.

To use the MacCormack scheme we consider the system in Eq. (16) in generalized conservation form,

$$\frac{\partial \boldsymbol{w}}{\partial t} + \frac{\partial \boldsymbol{f}}{\partial x} = \boldsymbol{g}, \tag{24}$$

where

$$\boldsymbol{w} = \begin{pmatrix} A \\ u \end{pmatrix}, \quad \boldsymbol{f} = \begin{pmatrix} Au \\ \frac{1}{2}u^2 + 2\frac{a_0^2}{u_0^2}\left(1 - \sqrt{\frac{A_{\text{rest}}}{A}}\right) \end{pmatrix},$$

and

$$\boldsymbol{g} = \begin{pmatrix} 0 \\ -\frac{\partial p_a}{\partial x} - \frac{2(\gamma+2)\pi}{\text{Re}}\frac{u}{A} \end{pmatrix}.$$

The left hand side of Eq. (24) expresses the overall change in the $\boldsymbol{w}$-quantity and the right hand side allows sources and sinks. The first step in the MacCormack scheme calculates a preliminary value of $\boldsymbol{w}_j^{n+1}$,

$$\boldsymbol{w}_j^{\overline{n+1}} = \boldsymbol{w}_j^n - \frac{\Delta t}{\Delta x}(\boldsymbol{f}_{j+1}^n - \boldsymbol{f}_j^n) + \Delta t \boldsymbol{g}_j^n, \tag{25}$$

where "the bar" over $(n+1)$ [the $(n+1)$th time step] indicates that it is an approximate value of $\boldsymbol{w}$ evaluated at the point $(j,n+1)$. Thus, the correction step is calculated as

$$\boldsymbol{w}_j^{n+1} = \frac{1}{2}(\boldsymbol{w}_j^n + \boldsymbol{w}_j^{\overline{n+1}}) - \frac{1}{2}\frac{\Delta t}{\Delta x}(\boldsymbol{f}_j^{\overline{n+1}} - \boldsymbol{f}_{j-1}^{\overline{n+1}}) + \Delta t \boldsymbol{g}_j^{\overline{n+1}}, \tag{26}$$

where $\boldsymbol{f}_j^{\overline{n+1}} = \boldsymbol{f}(\boldsymbol{w}_{j-1}^{\overline{n+1}})$ and $\boldsymbol{g}_j^{\overline{n+1}} = \boldsymbol{g}(\boldsymbol{w}_{j-1}^{\overline{n+1}})$.

The magnitude of the spatial and temporal step sizes was chosen so that the MacCormack scheme was stable. The difference equations are linearly stable if and only if $(\Delta t/\Delta x)\max|c_\pm| \le 1$.

Downloaded 05 Jan 2010 to 130.226.199.115. Redistribution subject to AIP license or copyright; see http://pof.aip.org/pof/copyright.jsp

V. PERIOD OF GRAVITATIONALLY DRIVEN OSCILLATIONS

In this section we address the question of why and how the fraction $D_k = D_{\text{tank}}/D_{\text{tube}}$ of the tank and tube cross-sectional areas, influences the period in the simple case of gravity driven oscillations, i.e., without pumping. For this analysis, we assume a constant tube radius corresponding to a nonelastic U-tube. Thus D_k is a constant parameter, i.e., independent of time and spatial variables, throughout this approach.

In the following we investigate a number of approaches and show that inclusion of a pressure loss term is essential for the formation of gravity driven waves. The resulting ODE allows us to estimate the period providing insight into the physics of the gravity driven oscillations. These estimates are calculated numerically from the model and they are confirmed analytically by perturbation theory.

We use the results of this simpler model to justify the results obtained with the distributed 1D model. Note that gravity is included in the distributed 1D model, where it appears in the boundary conditions and, as shown in Sec. VI, gravity plays an important role in the phenomenon of valveless pumping. In this section we therefore discuss the occurrence of oscillations due to gravity by a more complete analysis of the simpler model.

In literature much effort has been placed into modeling simple systems.[25] Without external compression our system is relatively simple but to our knowledge, there is only one other study of oscillations in the U-tube with spatial varying cross sections[26] analyzing gravitationally driven oscillations of a liquid column in a vertical pipe, open at both ends, and with the bottom immersed into a reservoir. Experimentally,[26] observe an eruption of a jet at the beginning of the rise of the water column, which in their experiment is caused by an initial singularity related to the zero mass of their oscillator. In their asymmetrical setup the mass of the oscillator changes constantly. In contrast to this, the mass of the system is constant and singularities related to eruption of jets do not appear in our system. Similar to the results presented in Ref. 26 we observe damped oscillations due to dissipation. However, as opposed to Ref. 26 we observe smooth damped sinuslike waves in experiments. This observation agrees with the symmetry of the governing equation, derived below. Due to the conservation of mass and the symmetry of the system we study, we are able to eliminate singular effects. Hence, the conclusions derived by Ref. 26 are not directly applicable for our study.

In conclusion, our goal in this section, is to estimate the period of the gravity driven oscillations formed when the system is started away from equilibrium. We derive a family of simple dynamical models that allows prediction of the period, and which provide us with insight into the mechanical effects. The correct way to do this is by using the integral form of the conservation of energy for the system. Hence, the rate of change in mechanic energy, i.e., kinetic and potential energies, equals the turbulent loss plus the viscous dissipation.[25] The turbulent loss is partly due to the elbows where flow and momentum change direction, i.e., where the tanks and tube meet, and partly to sudden changes in diameter (vena contracta) where fluid flows between tanks and tube. However, this approach is technically difficult, and we therefore present a more direct approach based on the momentum equation. Unfortunately this "mechanistic" approach has some loose ends. We account for these pitfalls by idealizing that the fluid moves in a 1D system only. This corresponds to neglecting the 90° turn at the elbows connecting the tank and the tube. Alternatively we may assume that the losses, due to transforming the vertical momentum to horizontal momentum and visa versa, are included in the turbulent loss applied at the sudden change in diameters between the tanks and the tube.

If the water level starts slightly above the equilibrium level, it is possible to ignore time and spatial variation in the tube radius; thus we assume that the radius of the tube is constant and that it equals the radius at hydrostatic pressure. Since the total mass of water in the tube and the tanks remains constant the momentum equation holds, i.e.,

$$\frac{dP}{dt} = F_{\text{visc}} + F_{\text{loss}} + F_{\text{grav}}, \tag{27}$$

where P denotes the total momentum. Let x be the deviation in water level of the left tank, $x(t) = h(t) - h_0$, between the actual height, $h(t)$, and the height at equilibrium, h_0. In Eq. (27) F_{grav} denotes the gravitational force acting on the system,

$$F_{\text{grav}} = -2A_{\text{tank}}\rho g x.$$

Furthermore, using the continuity equation the viscous force F_{visc} becomes

$$\begin{aligned} F_{\text{visc}} &= -8\pi\mu \\ &\quad \times \left((l_{\text{tank,left}} + l_{\text{tank,right}}) \left.\frac{dx}{dt}\right|_{\text{tank}} + l_{\text{tube}} \left.\frac{dx}{dt}\right|_{\text{tube}} \right) \\ &= -8\pi\mu (2h_0 + l_{\text{tube}} D_k^2) \frac{dx}{dt}, \end{aligned} \tag{28}$$

with $l_{\text{tank,left}} + l_{\text{tank,right}} = 2h_0$ (the sum of fluid levels in the tanks), l_{tube} is the tube length, and $dx/dt|_{\text{tube}}$ and $dx/dt = dx/dt|_{\text{tank}}$ are the fluid velocity in the tube and the tanks, respectively. D_k is the tank to tube diameter ratio. Finally, F_{loss} represents the additional force resulting from resistance due to the abrupt change in the diameter, where the tanks are connected to the tube (resistance from the friction between the fluid and the walls could be included in this term too, as well as the loss at the elbows). Following Ref. 25 we assume that F_{loss} is proportional to the square of the velocity but directed opposite the velocity, i.e.,

$$F_{\text{loss}} = -k_0(D_k)\rho \left|\frac{dx}{dt}\right| \frac{dx}{dt},$$

where the loss coefficient, k_0, depends on the ratio D_k.

Downloaded 05 Jan 2010 to 130.226.199.115. Redistribution subject to AIP license or copyright; see http://pof.aip.org/pof/copyright.jsp

In addition to this, the total momentum $P=P_{\text{tank,left}}+P_{\text{tank,right}}+P_{\text{tube}}$ is

$$P=(h_0+x)A_{\text{tank}}\rho\frac{dx}{dt}+(h_0-x)A_{\text{tank}}\rho\frac{dx}{dt}+l_{\text{tube}}A_{\text{tube}}\ \rho\frac{dx}{dt}\bigg|_{\text{tube}}=(2h_0+l_{\text{tube}})A_{\text{tube}}\rho D_k^2\frac{dx}{dt},$$

where the continuity equation has been used. Thus

$$\frac{dP}{dt}=m_e\frac{d^2x}{dt^2},$$

with m_e being the effective mass of the system

$$m_e=(2h_0+l_{\text{tube}})A_{\text{tube}}\rho D_k^2.$$

Hence Eq. (27) becomes

$$\frac{d^2x}{dt^2}+\frac{8\pi\mu(2h_0+l_{\text{tube}}D_k^2)}{(2h_0+l_{\text{tube}})A\rho D_k^2}\frac{dx}{dt}+\frac{k_0(D_k)}{(2h_0+l_{\text{tube}})AD_k^2}\left|\frac{dx}{dt}\right|\frac{dx}{dt}+\frac{2g}{2h_0+l_{\text{tube}}}x=0,\tag{29}$$

where $A=A_{\text{tube}}$.

If the two middle terms are ignored, which corresponds to disregarding viscosity and loss of energy, Eq. (29) describes a harmonic oscillator with period

$$T=2\pi\sqrt{\frac{2h_0+l_{\text{tube}}}{2g}}.\tag{30}$$

We note that T, in this approximation, becomes independent of D_k^2. This is intuitively absurd in the limit of vanishing tube diameter or infinite tank diameter, i.e., when $D_k^2\to\infty$. In the latter case an infinite amount of fluid has to move back and forward in a finite time T. Likewise in the limit $D_k^2\to 0$ one expects infinite damping to be important and that is not included in this approximation. Hence the approximation is useful only for $D_k^2\approx 1$.

If instead we ignore the loss term and include the viscous term, we obtain an equation describing the corresponding damped oscillator, $x(t)=x_0e^{-\gamma t}\cos(\omega t)$, with damping

$$\gamma=\frac{4\pi\mu(2h_0+l_{\text{tube}}D_k^2)}{(2h_0+l_{\text{tube}})A\rho D_k^2},\tag{31}$$

and frequency

$$\omega=\sqrt{\omega_0^2-\gamma^2}=\sqrt{\frac{2g}{2h_0+l_{\text{tube}}}-\left(\frac{4\pi\mu(2h_0+l_{\text{tube}}D_k^2)}{(2h_0+l_{\text{tube}})A\rho D_k^2}\right)^2}\tag{32}$$

for $\gamma<\omega_0$. From this equation one can see the effect of all the parameters analytically. Overdamping is observed in the limit $D_k^2\to 0$ as γ tends to infinity. However, in the limit where D_k tends to infinity loss becomes important. If it is not included, Eq. (32) predicts a finite period as in Eq. (30).

The above approximations do not give reasonable solutions in the limit $D_k\to\infty$. To improve this, we ignore the viscosity and include the loss term in Eq. (29). In order to continue, the loss coefficient $k_0(D_k)$ needs to be specified. In regions where the flow is laminar, $k_0(D_k)$ is normally assumed as proportional to D_k^2. More specifically, we let it depend on D_k^2-1 for symmetry reasons, which means that we only consider loss related to the abrupt change of diameters between the tube and tanks. For simplicity reasons we assume $k_0(D_k)=k(D_k^2-1)^2$, where k is the loss constant [in general, one can use a Taylor expansion $k_0(D_k)=k_2(D_k^2-1)^2+k_4(D_k^2-1)^4+\ldots$, omitting the odd powers due to symmetry, and the constant term due to the fact that the loss vanishes for $D_k=1$]. Hence, disregarding the viscosity term, Eq. (29) becomes

$$\frac{d^2x}{dt^2}+\frac{k/A(D_k^2-1)^2}{(2h_0+l_{\text{tube}})D_k^2}\left|\frac{dx}{dt}\right|\frac{dx}{dt}+\frac{2g}{2h_0+l_{\text{tube}}}x=0.\tag{33}$$

Note that the coefficient $\omega_0^2=2g/(2h_0+l_{\text{tube}})$ may be removed by the nondimensionalization of the time variable $s=\omega_0 t$. Thus the governing equation simplifies to

$$x''+\xi(D_k)|x'|x'+x=0,\tag{34}$$

where $\xi=\xi(D_k)=[k/(2h_0+l_{\text{tube}})A][(D_k^2-1)^2/D_k^2]$. The prime denotes the derivative with respect to s (i.e., $x'=dx/ds$, etc.). Thus the equation may be interpreted as a harmonic oscillator in the external force field,

$$F=-\xi(D_k)|x'|x'.$$

From this it follows that the total energy decreases with time:

$$E=\frac{1}{2}(x')^2+\frac{1}{2}x^2\Rightarrow\frac{dE}{ds}=x'x''+xx'=-\xi(D_k)|x'|(x')^2<0,\quad\forall\, x'\neq 0.$$

A consequence of this observation is that the trajectory will spiral toward a stable equilibrium point in the phase space.

Since we are interested in the cycle of the damped oscillation we rewrite Eq. (34) as a first order system of coupled differential equations. For this system we let $y=x'$ and then switch to polar coordinates, $x=r\cos(\theta)$ and $y=r\sin(\theta)$, in order to estimate the time it takes to change the angular variable by 2π. In polar coordinates,

$$\begin{aligned}r'&=-\xi(D_k)r^2|\sin(\theta)|\sin^2(\theta),\\ \theta'&=-1-\xi(D_k)r|\sin(\theta)|\sin(\theta)\cos(\theta),\end{aligned}\tag{35}$$

giving

$$\frac{dr}{d\theta}=\frac{\xi(D_k)r^2(\theta)|\sin(\theta)|\sin^2(\theta)}{1+\xi(D_k)r(\theta)|\sin(\theta)|\sin(\theta)\cos(\theta)}\approx\xi(D_k)r^2(\theta)|\sin(\theta)|\sin^2(\theta)+\mathrm{O}(\xi^2),\tag{36}$$

since $dr/d\theta=(dr/ds)/(d\theta/ds)=r'/\theta'$. For ξ small one may integrate the approximated expression explicitly to obtain the trajectory. For ξ sufficient small, regular perturbation theory to first order gives that the frequency is independent of ξ, which means that the cycle does not change with D_k in a neighborhood of $D_k=1$. Thus the derivative of the period with respect to D_k vanishes at $D_k=1$. From the governing equations in polar coordinates it follows that the exact period is

Downloaded 05 Jan 2010 to 130.226.199.115. Redistribution subject to AIP license or copyright; see http://pof.aip.org/pof/copyright.jsp

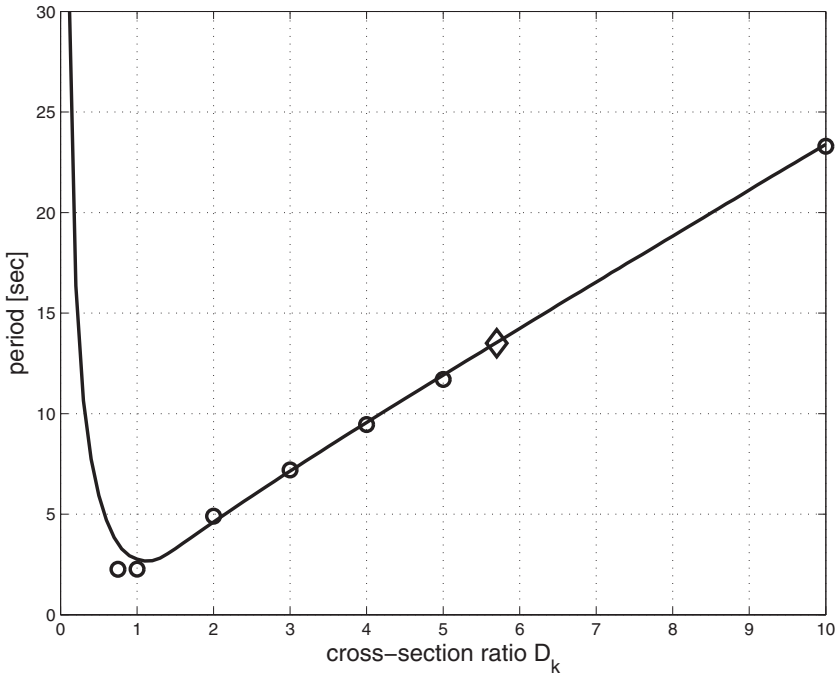

FIG. 3. Numerical results (solid curve) for the oscillation period as a function of D_k obtained from Eq. (35) by calculating how long time it takes for θ to increase by 2π. The loss coefficient is $k=0.14$. Results are compared to periods obtained by the 1D model (circles) and the experimental value (diamond).

$$T = \int_0^{2\pi} -\frac{dt}{d\theta} d\theta = \int_0^{2\pi} \frac{1/\omega_0}{1+\xi(D_k) r(\theta)|\sin(\theta)|\sin(\theta)\cos(\theta)} d\theta, \tag{37}$$

where $dt/d\theta = 1/(d\theta/dt) = 1/(\omega_0 \theta')$ and $r(\theta)$ is given by the differential Eq. (36). From the expressions in Eq. (35), the time for one revolution is calculated, i.e., the time it takes to increase θ by 2π. For D_k in a neighborhood of 1, the result agrees with the result mentioned above for ξ small but shows, in addition, that the D_k-dependence of the period becomes linearly increasing for large values of D_k. Furthermore, it shows that the period diverges in the limit $D_k \to 0$, as seen in Fig. 3 (full curve with $k=0.14$) of the results section.

VI. RESULTS

In this section we summarize results obtained from the models presented. The main focus will be on the distributed 1D model presented in Sec. III. Unless otherwise mentioned, the parameters in Table I are used in the numerical calculations.

A. Period of gravitationally driven oscillations

We start by comparing the distributed 1D model derived in Sec. III with the simpler models derived in Sec. V and with our experimental findings. This comparison allows us to validate the distributed 1D model and to gain more insight into the physics of the gravitationally driven oscillations.

Figure 3 shows the period calculated numerically (full curve) from Eq. (35) compared to the results obtained from the distributed 1D model (circles) (derived in Sec. III) and a single value measured experimentally (the diamond) (see Sec. II).

Note the close correspondence among the period obtained with the 1D model (to be studied further in Sec. VI B) 13.5 s, the period predicted by the simple model [Eq. (35)] 13.54 s, and the measured period 13.5 s. In Fig. 4 we compare an experimentally obtained time-series of water levels in one of the tanks and the model prediction based on the full Eq. (29) including both energy loss and viscosity.

TABLE I. Parameters used in the models and simulations. The values agree with those obtained from the experiment.

Gravity $g=9.81$ m/s^2
Constant external pressure $p_0=1.013\times10^5$ Pa
Density of water $\rho_{\text{water}}=998$ kg/m^3
Viscosity of water $\mu_{\text{water}}=0.001$ kg/s m
Rest diameter of tube $D_{\text{rest}}=0.03$ m
Rest diameter of tank $D_{\text{tank}}=D_k D_{\text{rest}}$
Tank/tube fraction $D_k=5.7$
Tube wall thickness $s=0.004$ m
Tube length $l_0=1.8$ m
Young modulus of tube $E=4.033\times10^6$ kg/m s^2
Loss constant $\xi=0.5$
Pump amplitude $\eta=1.68$
Pump region start $x_A=0.2l_0$
Pump region end $x_B=0.4l_0$
Water heights in the tanks at $t=0$ is $h_0=1$ m
Standard position of the pump $x_c=0.3l_0$
Characteristic velocity $u_0=0.2$ m/s
Characteristic length $r_0=0.015$ m (the rest radius of the tube)
Dimensionless time step $\Delta t=0.001$
Dimensionless space step $\Delta x=0.6$
Spatial tube divisions $J=200$
Loss coefficient $k=0.14$

Downloaded 05 Jan 2010 to 130.226.199.115. Redistribution subject to AIP license or copyright; see http://pof.aip.org/pof/copyright.jsp

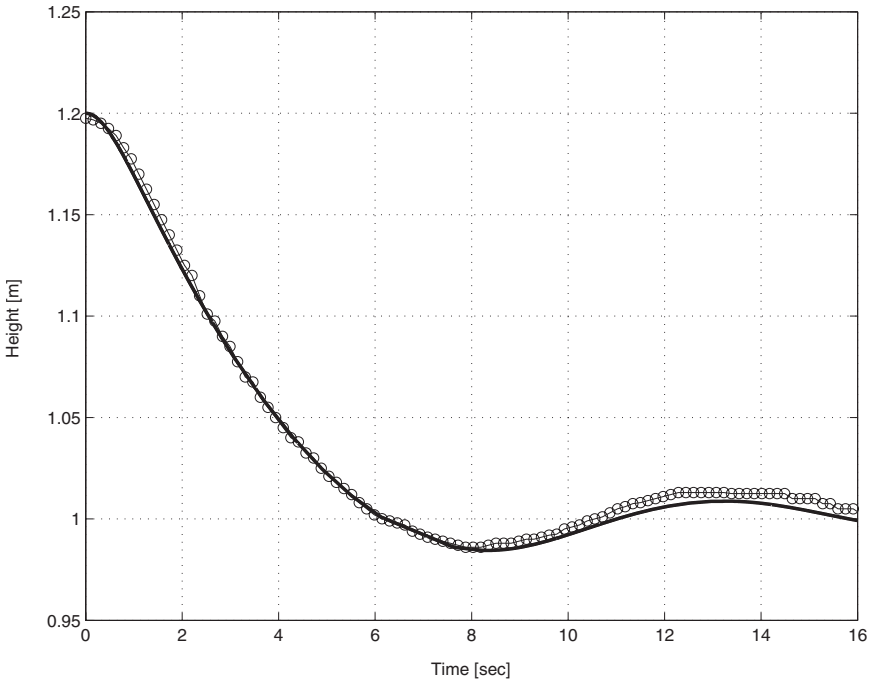

FIG. 4. Experimentally obtained data (circles) and model results (solid curve) of height vs time for the gravitationally driven damped oscillations in the U-tube system. The model is the simple model with viscosity, energy loss, and gravitation included as stated in Eq. (29).

Again a convincing agreement is observed between the experimental data and the full model. The period is estimated to 13.3 s, see the reed graph in Fig. 4. Finally, note that the viscosity term $\|8\pi\mu(2h_0+l_{\text{tube}}D_k^2)/(2h_0+l_{\text{tube}})A\rho D_k^2 dx/dt\|_\infty \approx 2\times10^{-4}$ m/s^2, that the loss term $\|k_0(D_k)/(2h_0+l_{\text{tube}})AD_k^2|dx/dt|dx/dt\|_\infty \approx 10^{-3}$ m/s^2, and that the gravity term $\|2g/(2h_0+l_{\text{tube}})x\|_\infty \approx 5\times10^{-2}$ m/s^2. Thus the approximation resulting in Eq. (33), and the analysis based on it, are justified.

B. Viscosity in the distributed 1D model

The use of the word simulation in the rest of this section refers to simulations by the dimensionless distributed 1D model derived in Sec. III. However, all results are presented in a dimensional form.

Figure 5 shows the difference between water levels in the two tanks as a function of time when the viscosity is zero. The results in the zoomed box are for the first 2.5 s. The pump is set at a frequency of 3.5 Hz and the oscillations due to the pump are visible in the zoomed box. Note that when the pump is active, the height difference between the two tanks deviates from zero if the pump is not placed at $0.5l_0$. Furthermore, if the viscosity is nonzero, the height difference reaches an oscillatory equilibrium state with a mean different from zero. If the viscosity is zero, the height difference oscillates between zero and a constant height difference determined by the pump, and the pump affects the amplitude of the gravity driven oscillations whereas the period is not affected. Gravity and the physical proportions of the system determine the oscillation period.

Deactivating the pump and changing the initial conditions to $\Delta h=0.1$ m make it possible to calculate the oscillation period caused by gravity. This results in a period of 13.5 s, which is close to the oscillation period of 13.35 s obtained when the pump is activated. So, these long period oscillations are an effect of gravity. Similar observations are briefly mentioned, but not documented in Ref. 10. In contrast to our findings, the numerical studies in Ref. 12 show damping even for zero viscosity. A possible explanation could be that it is essential to use the instationary Bernoulli equation in the derivation of the boundary conditions.

When viscosity is nonzero the gravitational oscillations are damped and the height difference reaches an oscillatory steady state. Figure 6 shows the oscillation phenomenon at four different values of the viscosity.

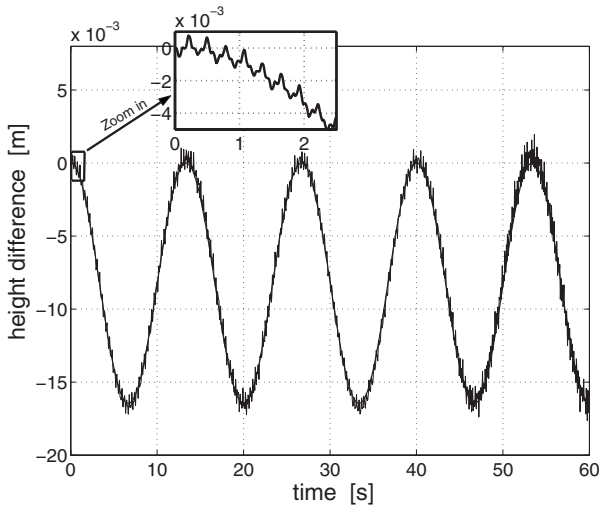

FIG. 5. Height difference between water levels in the tanks. Results from the distributed 1D model (rapid oscillating curve) have been fitted (solid curve) using the trigonometric function $f_{\text{fit}}(t)=(f_A/2)\{1-\cos[(2\pi/T)t]\}$, where f_A is twice the oscillation amplitude and T is the oscillation period. The maximum deviation from the zero height difference and oscillation period are $|f_A|=0.0165$ m and $T=13.35$ s, respectively. A zoomed box of the first 2.5 s of the simulation is inferred. The pump frequency is 3.5 Hz and it is clearly responsible for the small oscillations embedded in the oscillations with the longer period.

Downloaded 05 Jan 2010 to 130.226.199.115. Redistribution subject to AIP license or copyright; see http://pof.aip.org/pof/copyright.jsp

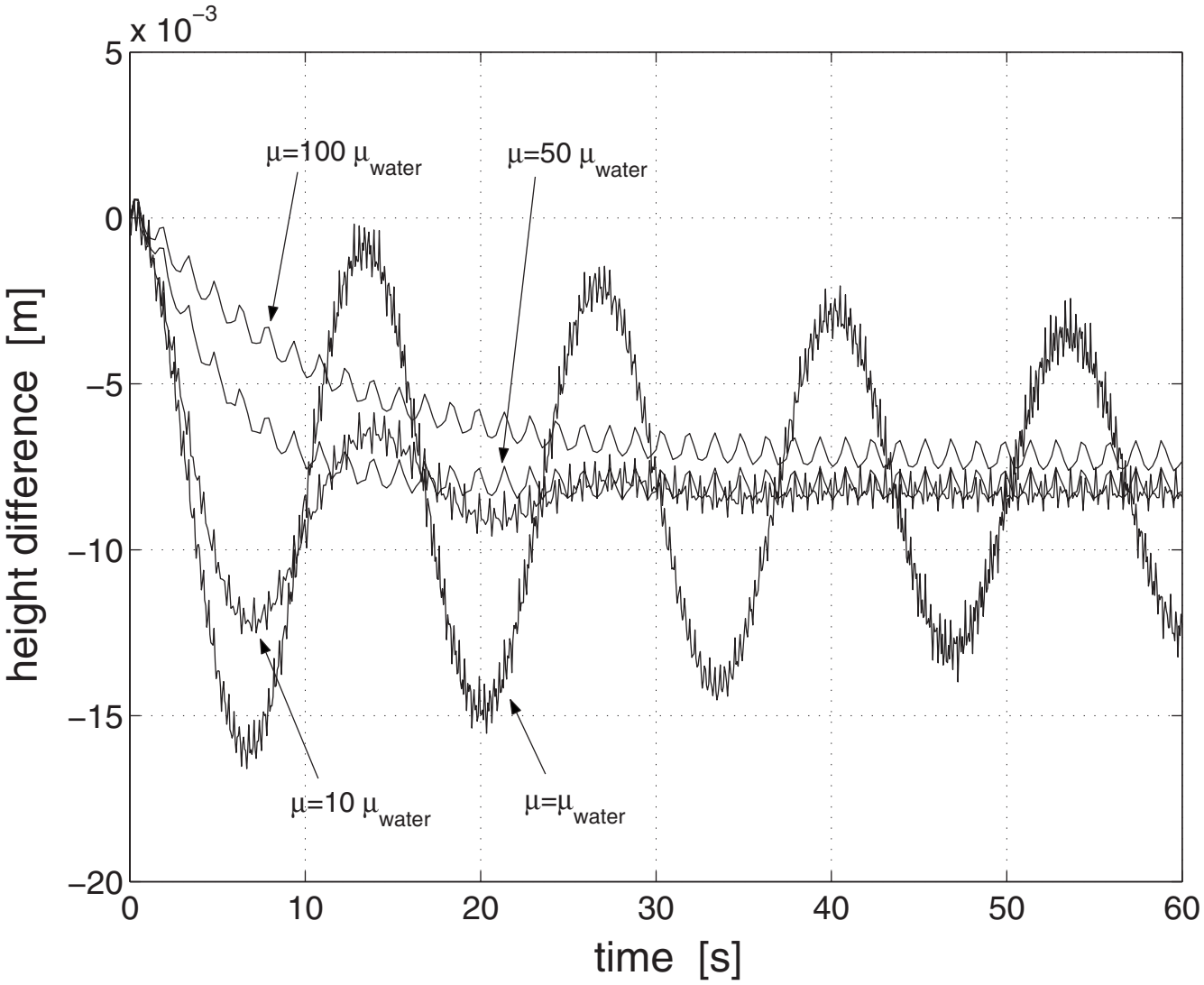

FIG. 6. Height difference between water levels in the tanks. Numerical simulations for four different values of viscosity; $\mu=\mu_{\text{water}}$, $\mu=10\mu_{\text{water}}$, $\mu=50\mu_{\text{water}}$, and $\mu=100\mu_{\text{water}}$. The pump frequency is 3.5 Hz. For clarity not all points are plotted for $\mu=50\mu_{\text{water}}$ and $\mu=100\mu_{\text{water}}$.

C. Frequency dependence

The frequency dependence of the height difference has been investigated in the frequency domain 0.5–15 Hz in steps of 0.5 Hz. At each frequency the height difference was calculated in the time domain 0–60 s. After the transient, the mean value was calculated by averaging over an integer number of oscillations (the number of oscillations depends on the frequency) and plotted versus frequency, as shown in Fig. 7 (asterisks).

The simulations show that the height difference changes with frequency, and that mean flow reversals occur, even when the point of compression is maintained. Furthermore, since the simulations diverge near frequencies of flow reversals, it is reasonable to assume that eigenfrequencies of the system play an important role in the valveless pumping. This hypothesis is underpinned by the observation that the numerical solutions become unstable at points of reversal if the viscosity is zero. This result also indicates that reversal occur when the pumping frequency collides with the resonance frequencies of the system. However it is not always the case that reversal is associated with resonance. Shifts in mean flow direction can also occur continuously. We term those points zero points, and points associated with resonance phenomenon are termed resonance points. The eigenfrequencies are analyzed further in Sec. VI E.

D. Pump position

Figure 7 shows that varying the pump position does not change the location of the resonance points, but it does influence the location of the zero points. Furthermore, the pump position also influences the mean water level difference. The largest absolute value of the water level difference is achieved when the pump is placed at one third of the tube length for frequency $\nu=14.84$ Hz (shown to be four times the fundamental eigenfrequency of the linearized system).

In order to examine the relationship between the pump position and the height difference, the pump position was varied while the pumping frequency was kept constant at a

Downloaded 05 Jan 2010 to 130.226.199.115. Redistribution subject to AIP license or copyright; see http://pof.aip.org/pof/copyright.jsp

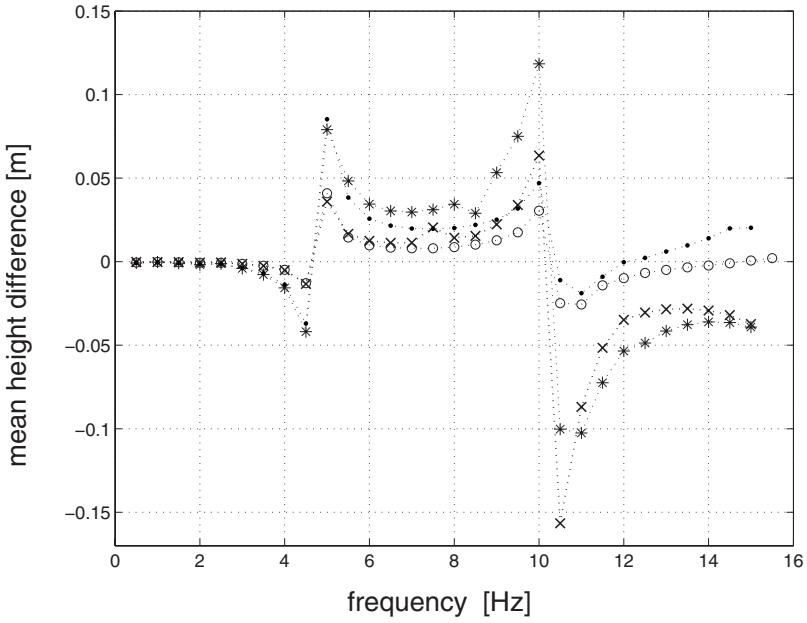

FIG. 7. Height difference between water levels in the tanks. Frequency scans at four different pump positions. At $x_c=0.3l_0$ and $x_c=0.4l_0$ (asterisks and crosses, respectively) flow reversals are due to resonance, while at $x_c=0.2l_0$ and $x_c=0.25l_0$ (dots and circles, respectively) the mean flow also reverses (at approximately 12 and 15 Hz) without any sign of resonance. Note that the pump position does not significantly affect the location of the resonance points, while it does affect the location of the zero points.

frequency where the wavelength of the oscillation equals the length of the tube. Results show the sinuslike wave shown in Fig. 8 (circles and dots).

As shown in Fig. 8, the height difference depends on the pump position in a nontrivial way. At a frequency of 14.84 Hz the height difference becomes zero when the pump is placed in the middle at $0.5l_0$ (as would be expected due to symmetry), but the difference also becomes zero when the pump is placed at $0.25l_0$ and at $0.75l_0$. When the pumping frequency is halved so that the wavelength of the pump frequency is $2l_0$, the difference becomes zero only when the pump is placed at $x_c=0.5l_0$. The transition from a two period wave to a one period wave has been investigated and the numerical results are shown in Fig. 8. Starting at $\nu=7.42$ Hz the mean height difference increases when the frequency is increased. After the resonance point at 10.5 Hz the mean height difference changes sign but retains, approximately, the same absolute value. A further increase in frequency reduces the mean height difference. The shift from one period waves to two period waves appears at the resonance point.

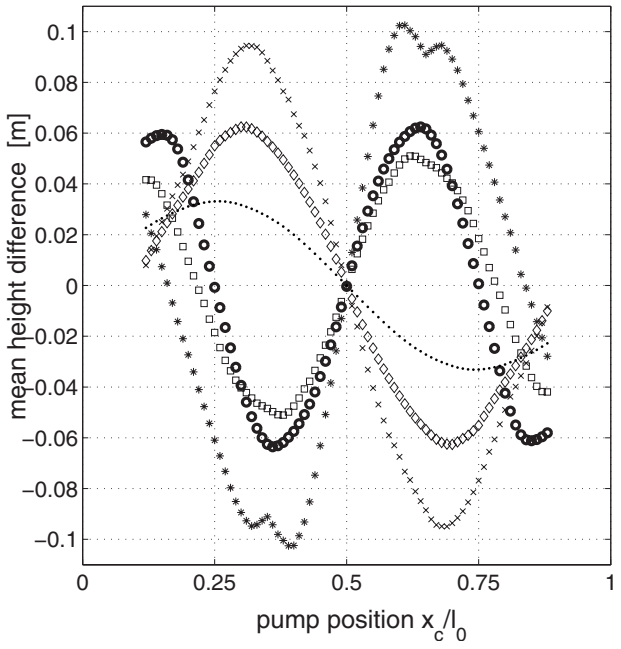

FIG. 8. Height difference between the water levels in the tanks. Position scans for frequencies 7.42,9.28,9.75,11.33,12.99, and 14.84 Hz (dots, diamonds, crosses, asterisks, circles, and squares, respectively). The resonance point lies close to 10.5 Hz.

E. Eigenfrequencies, resonance frequencies and horizontal slope frequencies by linearizing

Linearizing of the 1D model derived in Sec. III can be used to get an approximate theoretical explanation for the frequencies of the resonance points and of the points of horizontal slope, see Fig. 7. In the following, these frequencies are termed resonance frequencies and horizontal slope frequencies, respectively. Furthermore, a justification for the choice of pumping frequencies, $\nu=14.84$ and $\nu=7.42$, is given based on the present analysis.

The resonance frequencies agree well with the eigenfrequencies of the linearized system with asymmetric boundary conditions. Horizontal slope frequencies agree with the eigenfrequencies of the linearized system but with symmetric boundary conditions.

Linearizing Eq. (4), near points where $A=A_{\text{rest}}$ and $u=0$ (i.e., no flow) and without pumping, gives a wave equation for u,

$$\frac{1}{a_0^2}\left(\frac{\partial^2 u}{\partial t^2}+b\frac{\partial u}{\partial t}\right)-\frac{\partial^2 u}{\partial x^2}=0, \tag{38}$$

with a_0 as the wave velocity at $A=A_{\text{rest}}$ and $b=2\pi\mu(\gamma+2)/(\rho A_{\text{rest}})$ representing the attenuation.

The eigenfrequencies of the linearized system, near vanishing mean flow, fulfilling the symmetric boundary conditions $u(t,0)=u(t,l_0)=0$ or $\partial u/\partial t(t,0)=\partial u/\partial t(t,l_0)=0$ give the horizontal slope frequencies,

Downloaded 05 Jan 2010 to 130.226.199.115. Redistribution subject to AIP license or copyright; see http://pof.aip.org/pof/copyright.jsp

$$\nu_n = \sqrt{n^2\left(\frac{a_0}{2l_0}\right)^2 - \left(\frac{b}{2}\right)^2} \approx n\frac{a_0}{2l_0}$$
$$= \{7.42, 14.84, 22.25, 29.66, \ldots\}, \quad (39)$$

for $n \in \mathbf{Z}_+$. The approximation appearing in Eq. (39) is suitable given our choice of parameter values. These frequencies, corresponding to symmetric boundary conditions, describe the situations where the same amount of energy flows across the two boundaries. More precisely, the first boundary condition (nodes at both boundaries) corresponds to the situation where no energy flows across the boundaries; the second corresponds to the situation in which the same amount of energy crosses the two boundaries. In Fig. 7 these are the points with horizontal tangents (approximately at 7.5 and 14 Hz). At these points, the absolute value of the height difference has a local minima. The horizontal slope frequencies are also demonstrated in Fig. 8, where sinuslike waves with nodes at the boundaries appear at frequencies corresponding to a tube length of multiple of half a wavelength.

The eigenfrequencies of the linearized system near vanishing mean flow fulfilling the asymmetric boundary conditions $u(t,0)=\partial u/\partial t(t,l_0)=0$ or $\partial u/\partial t(t,0)=u(t,l_0)=0$ gives the resonance frequencies,

$$\nu_n = \sqrt{\left(n+\frac{1}{2}\right)^2\left(\frac{a_0}{2l_0}\right)^2 - \left(\frac{b}{2}\right)^2} \approx \left(n+\frac{1}{2}\right)\frac{a_0}{2l_0}$$
$$= \{3.71, 11.13, 18.55, 25.97, \ldots\} \quad (40)$$

for $n \in \mathbf{Z}_+ \cup \{0\}$. Again the approximation made in Eq. (40) is suitable given our choice of parameter values. These frequencies, corresponding to asymmetric boundary conditions, describe the situations of changing flow. More specifically, the two sets of asymmetric boundary conditions correspond to situations where maximum energy is transported across one boundary (the one where the antinode is) and nothing across the other (the one where the node is). In Fig. 7 these are the points of resonance, located approximately at 4.5 and 10.5 Hz. Hence, resonance appear where the solutions have a node at one end and an antinode at the other, corresponding to a tube length of multiple of a quarter of a wavelength. Similar observations can also be extracted from the numerical simulations by Ref. 14 and those by Ref. 4.

F. Nonlinear description of resonance points

In this subsection we consider the nonlinearized 1D model. As regard the full system, it should be noted that changing the length of the tube affects the location of both the resonance points and the zero points in a manner not exactly as predicted by the linearized model described in Sec. VI E. If the locations of the first and the second resonance points are plotted against the length of the tube, the relationship follows a power law, although not the same power law for both resonance points, see the upper panels of Fig. 9.

If the frequencies of the first and second resonance points are denoted f_{r1} and f_{r2}, respectively, the numerical results give the following relations:

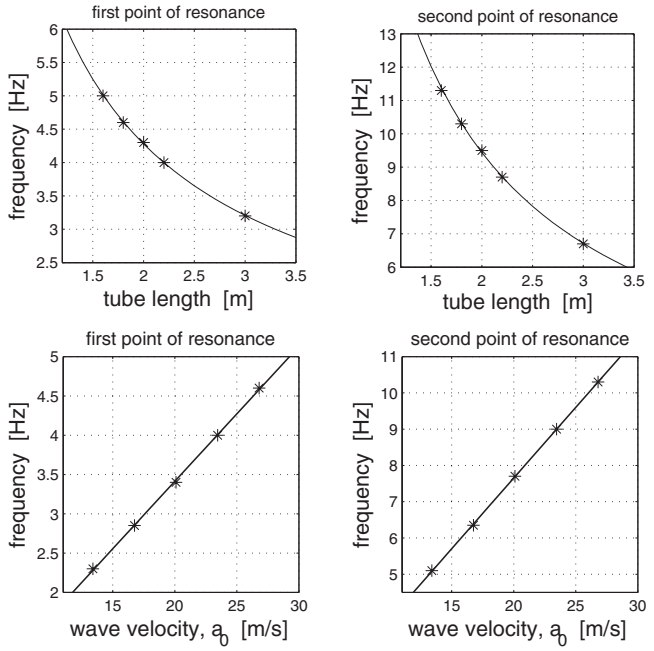

FIG. 9. Upper panels: the resonance frequencies (asterisks) plotted against the length of the tube for the first (left graph) and second (right graph) point of resonance. Five different lengths have been used: $l_0=1.6$, 1.8, 2, 2.2, and 3 m. The viscosity is $\mu=\mu_{\text{water}}$ and the wave propagation velocity is $a_0=26.8$ m/s. The curves represent best fit by power laws. Lower panels: the resonance frequencies (asterisks) plotted against the wave propagation velocity for the first (left graph) and second (right graph) resonance point. Note that the frequency and the wave velocity are proportional. The length of the tube is fixed at $l_0=1.8$ m.

$$f_{r1} = 7l_0^{-3/4} \quad \text{and} \quad f_{r2} = 16.9l_0^{-0.84}. \quad (41)$$

The wave propagation velocity is determined by the model parameters: $a=\sqrt{(4/3)(sE/\rho D_{\text{rest}})}\sqrt[4]{A_{\text{rest}}/A}=a_0\sqrt[4]{A_{\text{rest}}/A}$. Note that the constant a_0 is the only place where the density, the tube wall thickness, and the Young modulus enter the equations. Thus, these quantities can be combined into one parameter and instead of changing each one of them and analyze the results, it is sufficient to change the wave velocity constant a_0 and study how the locations of the resonance frequencies are affected.

Frequencies of the first and second resonance points as a function of the wave propagation velocity can be seen in the lower panel of Fig. 9. The numerical results give the following relations for the first and second resonance point:

$$f_{r1} = 0.17a_0 \quad \text{and} \quad f_{r2} = 0.38a_0. \quad (42)$$

Based on the relations in Eqs. (41) and (42) we make the conjecture that the following relations between the resonance points, the length of the tube, and the wave propagation velocity hold:

$$f_{r1} = k_1\frac{a_0}{l_0^{3/4}} \quad \text{and} \quad f_{r2} = k_2\frac{a_0}{l_0^{0.84}}. \quad (43)$$

As to the first resonance point we get from Eq. (41) that $k_1=0.261$ and from Eq. (42) that $k_1=0.264$. For the second resonance point a similar calculation can be made. From Eq. (41) the constant can be calculated to $k_2=0.631$ and from Eq. (42) the calculation gives $k_2=0.623$.

Downloaded 05 Jan 2010 to 130.226.199.115. Redistribution subject to AIP license or copyright; see http://pof.aip.org/pof/copyright.jsp

Regression analysis between estimated first and second resonance frequency (based on simulations) and a_0/l_0^m (where $m=3/4$ for the first resonance point and $m=0.84$ for the second resonance point) over 25 points (all combinations of $a_0=13.4$; 16.8; 20.1; 23.4; 26.8 and $l_0=1.6$; 1.8; 2.0; 2.2; 3.0) gives the following relationships between the locations of the first resonance point, the second resonance point, and the wave propagation velocity and the length of the tube:

$$f_{r1}=0.26\frac{a_0}{l_0^{3/4}} \quad \text{and} \quad f_{r2}=0.63\frac{a_0}{l_0^{0.84}}, \tag{44}$$

i.e., regression analysis gives $k_1=0.26\pm0.01$ and $k_2=0.63\pm0.01$.

VII. SUMMARY AND CONCLUDING REMARKS

A. The instationary Bernoulli equation

In this paper we have shown that the instationary Bernoulli equation serves as a natural boundary condition for the tube-tank valveless flow problem. The modeling results are in qualitative agreement with those reported by others:[12,10] The average flow direction and the size of the flow are very sensitive to the pumping frequency, and the results show that valveless pumping occurs in the system.

B. Frequency dependence and nodes

We have shown that the height difference, generated by the average flow, varies in a systematical way with the position of the pump along the tube. This has also been noticed in Ref. 12. We showed that this variation constitute a spatial symmetric one-node sinuslike curve [i.e., $h_{\text{mean}}(x)=C\sin(2\pi x/l_0)$ for some constant C] for pump frequency $\nu=7.42$ Hz. We also showed that vanishing height difference (no mean flow) occur when the pump is positioned at $0.5l_0$ (or at the ends). We noted that the frequency $\nu=7.42$ Hz corresponds to the first horizontal slope frequency $\nu_1=a_0/2l_0$ of the tube. Furthermore, when the frequency is doubled, $\nu=2\nu_1=14.84$ Hz, the "period" of the sinuslike curve also "doubles" to a symmetric three-node sinuslike curve [i.e., $h_{\text{mean}}(x)=C\sin(4\pi x/l_0)$ for some constant C]. Hence, the height difference is zero when the pump is positioned at $0.5l_0$, $0.25l_0$, and $0.75l_0$ (or at the ends). In between the two pumping frequencies ν_1 and $\nu_2=2\nu_1$ there is a resonance point (near $\nu=10.5$ Hz). When the pump frequency varies from the one-node frequency to the three-node frequency the curve varies in a characteristic way: First, the amplitude of the sinuslike curve increases and diverges at the resonance frequency. Second, when passing the resonance frequency the sign of the amplitude changes, i.e., the curve is reflected, and the shift from one node to three nodes appears.

C. Flow reversal and resonance

A new observation, apparently, is that at least two different characteristic flow reversals may exist. As mentioned, we saw resonance points in the frequency spectrum, but we also observed more smoothly appearing transitions. We denoted these point resonance points and zero points. We used simulations to show that the resonance points do not depend on the pump position whereas the zero points do.

D. Experimental findings

A physical realization of the system has been constructed and some experiments have been carried out, see Sec. II. The experimental findings resemble the numerical results reported in this paper, such as height differences caused by pumping and flow reversals at resonance points. Recordings of the system can be found at the online version by clicking on Fig. 1.

E. Gravity driven oscillations

Special attention was devoted to gravity driven oscillations (without pumping) and the implication of the losses due to changes in the cross-sectional area between the tube and the tanks. A simpler model was developed ignoring time variation in the cross-sectional area of the tube. We found that it is necessary to account for the energy loss in order to have a physically acceptable dependence on the period of the resulting oscillations, and that the period is asymptotically linear in the tank to tube diameter ratio. We note that for realistic values of viscosity one may identify a pronounced gravity component in the 1D model simulations. This pronounced gravity component was excellently fitted by a cosine function. The simpler model for studying the period of the gravity driven oscillations agreed excellently with the periods predicted by the 1D model and with the experimental values.

F. Relation between resonance, tube length, and wave propagation velocity

Using the linearized 1D model in Eq. (38) in Sec. VI E, we predicted a set of eigenfrequencies. These frequencies constitute the resonance frequencies and the horizontal slope frequencies. The resonance frequencies are related to asymmetric boundary conditions, and horizontal slope frequencies are related to symmetric boundary conditions. The fundamental eigenfrequency $\nu_1=3.71$, and the higher order eigenfrequencies $\nu_2=11.13$, $\nu_3=18.55$, $\nu_4=25.97$, etc., given by Eq. (40) are approximately equal to the resonance frequencies, where the reversals of flow occur (see Fig. 7 of Sec. VI C). The horizontal slope frequencies $\nu_1=7.42$, $\nu_2=14.84$, $\nu_3=22.25$, $\nu_4=29.66$, etc., given by Eq. (39) are in precise agreement with the one-node and the three-node sinuslike waves discussed in Sec. VI D. Another important discovery is that the nonlinear 1D model predicts a refinement of the resonance frequencies predicted by linearization. In fact, there seems to be a simple linear relationship between the first resonance point and a certain power of the (inverse) tube length. The frequency of the first resonance point is proportional to the wave propagation velocity divided by the tube length to the power 0.75 with proportionality constant 0.26. We found a similar relation for the frequency of the second resonance point but with power 0.84 and proportionality constant 0.63. Based on these two findings we hypothesize that it is possible to relate the first and the second resonance

Downloaded 05 Jan 2010 to 130.226.199.115. Redistribution subject to AIP license or copyright; see http://pof.aip.org/pof/copyright.jsp

frequencies. It deserves to be mentioned that the power deviates significantly from one—the expected value. The discrepancies between the linearized estimates and those estimated from the nonlinear 1D model are 20% and 8%, respectively. Further investigations into this discrepancy are needed.

[1]H. Thomann, "Simple pumping mechanism in a valveless tube," Z. Angew. Math. Phys. **29**, 169 (1978).
[2]M. Moser, J. Huang, G. Schwarz, T. Kenner, and A. Noordergraaf, "Impedance defined flow. Generalisation of William Harvey's concept of the circulation: 370 years later," Int. J. Cardiovasc. Med. Sci. **1**, 205 (1998).
[3]E. Jung, "2-D Simulations of valveless pumping using the immersed boundary method," Ph.D. thesis, New York University, 1999.
[4]E. Jung and C. Peskin, "Two-dimensional simulations of valveless pumping using the immersed boundary method," SIAM J. Sci. Comput. (USA) **23**, 19 (2001).
[5]J. T. Ottesen, "Valveless pumping in a fluid-filled closed elastic tube-system: One-dimensional theory with experimental validation," J. Math. Biol. **46**, 309 (2003).
[6]J. T. Ottesen, "Symmetric compressions of a fluid filled torus of asymmetric elasticity generates mean flow of frequency dependent size and orientation," *Mathematical Modelling and Computing in Biology and Medicine*, edited by V. Capasso (Progetto Leonardo ESCULAPIO, Bologna, Italy, 2003), pp. 235–241.
[7]C. Manopoulos, D. Mathioulakis, and S. Tsangaris, "One-dimensional model of valveless pumping in a closed loop and numerical solution," Phys. Fluids **18**, 017106 (2006).
[8]J. Hansen, J. T. Ottesen, and A. Lemarchand, "Molecular dynamics simulations of valveless pumping in a closed microfluidic tube-system," Mol. Simul. **31**, 963 (2005).
[9]J. Hansen and J. T. Ottesen, "Molecular dynamics simulations of oscillatory flows in microfluidic channels," Microfluid. Nanofluid. **2**, 301 (2006).
[10]H. Rath, "Berechnungen zu einem ventillosen Pumpprinzip" Ph.D. dissertation, Technischen Universität, 1976.
[11]H. Rath and I. Teipel, "Der Fördereffekt in ventillosen, elastischen Leitungen," Z. Angew. Math. Phys. **29**, 123 (1978).
[12]A. Borzi and G. Propst, "Numerical investigation of the Liebau phenomenon," ZAMP **54**, 1050 (2003).
[13]S. Timmermann, "Matematisk modellering af vaeskestroemningen i elastisk forbudne kar med periodisk sammenpresning," M.S. thesis, Roskilde University, 2004.
[14]A. Hickerson and M. Gharib, "On the resonance of a pliant tube as a mechanism for valveless pumping," J. Fluid Mech. **555**, 141 (2006).
[15]S. Takagi and K. Takahashi, "Study of a piston pump without valves," Bull. JSME **28**, 831 (1985).
[16]G. Propst, "Pumping effects in models of periodically forced flow configurations," Physica D **217**, 193 (2006).
[17]M. Olufsen, "Modeling the arterial system with reference to an anestesia simulator," Ph.D. thesis, Roskilde University, 1998.
[18]J. Lighthill, *Mathematical Biofluiddynamics* (SIAM, Philadelphia, 1975).
[19]R. Panton, *Incompressible Flow* (Wiley, New York, 1996).
[20]S. Takagi and T. Saijo, "Study of a piston pump without valves," Bull. JSME **26**, 1366 (1983).
[21]S. Canic, "Blood flow through compliant vessels after endovascular repair: wall deformations induced by the discontinuous wall properties," Comput. Visualization Sci. **4**, 147 (2002).
[22]R. MacCormack, "The effect of viscosity in hypervelocity impact cratering," AIAA Hypervelocity Impact Conference, 1969, Paper No. 69-354, pp. 1–7.
[23]F. Casadei, G. Fotia, E. Gabellini, F. Maggio, and A. Quarteroni, "A mortar spectral/finite element method for complex 2d and 3d elastodynamic problems," Comput. Methods Appl. Mech. Eng. **191**, 5119 (2002).
[24]J. deFrutos, B. García-Archilla, and J. Novo, "The postprocessed mixed finite-element method for the Navier–Stokes equations: Refined error bounds," SIAM (Soc. Ind. Appl. Math.) J. Numer. Anal. **46**, 201 (2007).
[25]R. Granger, *Fluid Mechanics* (Dover, New York, 1995).
[26]E. Lorenceau, D. Quere, J.-Y. Ollitrault, and C. Clanet, "Gravitational oscillations of a liquid column," Phys. Fluids **14**, 1985 (2002).

Downloaded 05 Jan 2010 to 130.226.199.115. Redistribution subject to AIP license or copyright; see http://pof.aip.org/pof/copyright.jsp